

# Band Structure of the Growth Rate of the Two-Stream Instability of an Electron Beam Propagating in a Bounded Plasma

I. D. Kaganovich<sup>a</sup> and D. Sydorenko<sup>b</sup>

<sup>a</sup>*Princeton Plasma Physics Laboratory, Princeton University, Princeton, New Jersey 08543, USA*

<sup>b</sup>*University of Alberta, Edmonton, Alberta T6G 2E1, Canada*

This paper presents a study of the two-stream instability of an electron beam propagating in a finite-size plasma placed between two electrodes. It is shown that the growth rate in such a system is much smaller than that of an infinite plasma or a finite size plasma with periodic boundary conditions. Even if the width of the plasma matches the resonance condition for a standing wave, a spatially growing wave is excited instead with the growth rate small compared to that of the standing wave in a periodic system. The approximate expression for this growth rate is  $\gamma \approx (1/13)\omega_{pe}(n_b/n_p)(L\omega_{pe}/v_b)\ln(L\omega_{pe}/v_b)[1 - 0.18\cos(L\omega_{pe}/v_b + \pi/2)]$ , where  $\omega_{pe}$  is the electron plasma frequency,  $n_b$  and  $n_p$  are the beam and the plasma densities, respectively,  $v_b$  is the beam velocity, and  $L$  is the plasma width. The frequency, wave number and the spatial and temporal growth rates as functions of the plasma size exhibit band structure.

PACS numbers: 52.35.Qz, 52.40.Mj, 52.65.-y, 52.77.-j

Interaction of electron beams with plasmas is of considerable importance for many plasma applications where electron emission occurs from surfaces. The electrons extracted from the surface and accelerated in the sheath form a beam of electrons; the beam propagating in the plasma excites electron plasma waves through the two-stream instability [1]. Laboratory plasmas and plasmas in industrial applications are usually bounded by electrodes. We show that electrodes greatly affect the growth of the two-stream instability. Though beam-plasma systems have been studied extensively in the past using kinetic simulations, see *e.g.* [2], [3], [4], [5] the presence of electrically connected boundaries changes the character of the two-stream instability from convective to absolute, similar to the instability of a Pierce diode [6]. In the Pierce diode, the instability was studied extensively taking only beam electrons and neutralizing ions into account as relevant to vacuum diodes, see *e.g.* [7] and the references within. Here, we consider the two-stream instability between a low density electron beam and high density plasma electrons as relevant to discharges. In this Letter, we have performed an analytical study and fluid and particle-in-cell simulations in order to obtain the growth rate of the two-stream instability in a finite plasma bounded by electrically connected electrodes. To the best of our knowledge and to some extent to our surprise the solution to this problem was not reported before.

The linear stage of the instability can be described making use of fluid formalism which includes the continuity equations

$$\frac{\partial n_{e,b}}{\partial t} + \frac{\partial v_{e,b}n_{e,b}}{\partial x} = 0, \quad (1)$$

the momentum equations

$$\frac{\partial v_{e,b}}{\partial t} + v_{e,b}\frac{\partial v_{e,b}}{\partial x} = -\frac{e}{m}E, \quad (2)$$

and the Poisson equation

$$\frac{\partial^2 \phi}{\partial x^2} = 4\pi e(n_e + n_b - n_i), \quad (3)$$

where  $n_{e,b}$  and  $v_{e,b}$  are the densities and the velocities of the plasma and beam electrons,  $-e$  and  $m$  are the electron charge and mass,  $E = -\partial\phi/\partial x$  is the electric field,  $\phi$  is the electric potential, and  $n_i$  is the ion density. The initial plasma state is neutral:  $n_{e,0} + n_{b,0} = n_{i,0}$ , where  $n_{e,0}$  and  $n_{b,0}$  are the initial densities of the bulk and the beam electrons, and  $n_{i,0}$  is the initial density of ions, respectively. The ion density is uniform and constant,  $n_i = n_{i,0} = \text{const}$ . Initially, the bulk and the beam electron densities and the beam flow velocity are uniform everywhere. Note that everywhere in this paper subscripts  $e$  and  $b$  denote values related to plasma and beam electrons, respectively.

For the studies described in the present paper, the boundary conditions are non-periodic and describe a plasma produced in a discharge between two electrodes. At the ends of the system  $x = 0$  and  $x = L$ , the potential perturbations are set to zero,  $\phi(0) = \phi(L) = 0$ . The beam is injected at the boundary  $x = 0$ . The boundary conditions for the beam electrons are  $n_b(0) = n_{b,0}$  and  $v_b(0) = v_{b,0}$ , where  $v_{b,0}$  is the injection velocity of the beam. Note that in fluid simulations, a small sheath forms near the electrodes and more accurate boundary conditions are required to account for the sheath effect [13].

## Analytical Solution

The dispersion equation is obtained by solving linearized Eqs. (1-3) for perturbations of plasma and beam electron densities and velocities. The perturbations are

defined as

$$\begin{aligned}\delta n_e &= n_e - n_{e,0}, \quad \delta n_b = n_b - n_{b,0}, \\ \delta v_b &= v_b - v_{b,0}, \quad \delta v_e = v_e.\end{aligned}$$

Linearized equations can be readily solved using Laplace's method [8]. However, we are only looking for an asymptotic solution which the system approaches on longer times. Following the Pierce method [6], the asymptotic solution for the potential has the following form:

$$\delta\phi(t, x) = (Ax + Be^{ik_+x} + Ce^{ik_-x} + D)e^{-i\omega t}, \quad (4)$$

where  $\omega$  is the frequency of the wave,  $k_{\pm}$  are the wave vectors of the two waves propagating in the system, and coefficients  $A, B, C, D$  are complex constants. The density and the velocity perturbations are

$$\begin{aligned}\delta n_{e,b}(t, x) &= (\delta n'_{e,b} + \delta n_{e,b}^+ e^{ik_+x} + \delta n_{e,b}^- e^{ik_-x}) e^{-i\omega t}, \\ \delta v_{e,b}(t, x) &= (\delta v'_{e,b} + \delta v_{e,b}^+ e^{ik_+x} + \delta v_{e,b}^- e^{ik_-x}) e^{-i\omega t},\end{aligned} \quad (5)$$

The linearized equations for the parts of the perturbations proportional to  $\exp(-i\omega t + ik_{\pm}x)$  are

$$\begin{aligned}-i\omega\delta n_e^{\pm} + ik_{\pm}\delta v_e^{\pm} n_{e,0} &= 0, \\ -i\omega\delta v_e^{\pm} &= \frac{e}{m} ik_{\pm}\delta\phi^{\pm}, \\ -i\omega\delta n_b^{\pm} + ik_{\pm}(\delta v_b^{\pm} n_{b,0} + v_{b,0}\delta n_b^{\pm}) &= 0, \\ (-i\omega + ik_{\pm}v_{b,0})\delta v_b^{\pm} &= \frac{e}{m} ik_{\pm}\delta\phi^{\pm}, \\ -k_{\pm}^2\delta\phi^{\pm} &= 4\pi e(\delta n_e^{\pm} + \delta n_b^{\pm}),\end{aligned}$$

where  $\delta\phi^+ = B$  and  $\delta\phi^- = C$ . These equations yield:

$$\begin{aligned}\delta v_e^{\pm} &= \frac{\omega}{k} \frac{\delta n_e^{\pm}}{n_{e,0}}, \quad \frac{\delta n_e^{\pm}}{n_{e,0}} = -\frac{e}{m} \frac{k_{\pm}^2}{\omega^2} \delta\phi^{\pm}, \\ \delta v_b^{\pm} &= \frac{\omega - v_{b,0}k_{\pm}}{k_{\pm}} \frac{\delta n_b^{\pm}}{n_{b,0}}, \quad \frac{\delta n_b^{\pm}}{n_{b,0}} = -\frac{e}{m} \frac{k_{\pm}^2}{(\omega - kv_{b,0})^2} \delta\phi^{\pm}.\end{aligned} \quad (6)$$

Substitution of relations (6) into the Poisson equation gives usual dispersion relation for waves

$$1 = \frac{\omega_{e,0}^2}{\omega^2} + \frac{\omega_{b,0}^2}{(\omega - v_{b,0}k_{\pm})^2}. \quad (7)$$

Here  $\omega_{e,0}^2 \equiv 4\pi e^2 n_{e,0}/m$  and  $\omega_{b,0}^2 \equiv 4\pi e^2 n_{b,0}/m$  are the electron plasma frequencies corresponding to the plasma and beam densities.

The uniform parts of the density and velocity perturbations (5), which are proportional to  $\exp(-i\omega t)$  and correspond to high-frequency uniform electric field given by the first term in Eq. (4), are obtained in a similar way:

$$\delta v'_e = \delta v'_b = \frac{ie}{\omega m} A, \quad \delta n'_e = \delta n'_b = 0. \quad (8)$$

These perturbations correspond to high-frequency current flowing through the plasma and allow for  $\delta v_e \neq 0$  at the systems ends;  $\delta v_b(0) = 0$  because beam is injected with a given velocity but  $\delta v_b(L) \neq 0$ .

Applying four boundary conditions  $\delta n_b(0) = \delta v_b(0) = \delta\phi(0) = \delta\phi(L) = 0$  to perturbations (4) and (5) and taking into account (6) and (7) in the form

$$\omega - k_{\pm}v_{b,0} = \pm \frac{\omega_{b,0}}{\sqrt{1 - \frac{\omega_{e,0}^2}{\omega^2}}} \quad (9)$$

gives the following additional relation between  $\omega$  and  $k$ :

$$\begin{aligned}k_-^2 (e^{ik_+L} - 1) - \frac{ik_-^2 k_+ \omega L}{\omega - k_+ v_{b,0}} &= \\ k_+^2 (e^{ik_-L} - 1) - \frac{ik_+^2 k_- \omega L}{\omega - k_- v_{b,0}}.\end{aligned} \quad (10)$$

Eqs. (9) and (10) determine the temporal  $[\text{Im}(\omega)]$  and the spatial  $[\text{Im}(k)]$  growth rates of the instability as well as the frequency  $[\text{Re}(\omega)]$  and the wavenumber  $[\text{Re}(k)]$ . If plasma electrons are absent and only beam electrons are taken into account ( $n_{e,0} = 0$ ), Eq. (10) reduces to the Pierce's dispersion relation for vacuum diode.

In order to solve the dispersion relation (10), we introduce a new dimensionless variable

$$\chi = \frac{\omega_{b,0}/\omega_{e,0}}{\sqrt{1 - \frac{\omega_{e,0}^2}{\omega^2}}}. \quad (11)$$

Substituting (11) into (9) and assuming that  $\omega = \omega_{e,0}$  in the left-hand side of (9) gives

$$k_{\pm} = (1 \mp \chi) \frac{\omega_{e,0}}{v_{b,0}}. \quad (12)$$

Substitution (12) into (10) yields equation for  $\chi$

$$\begin{aligned}-i \frac{2(1-\chi)}{(1+\chi)\chi} L_n + e^{i(1-\chi)L_n} - 1 - \\ \frac{(1-\chi)^2}{(1+\chi)^2} [e^{i(1+\chi)L_n} - 1] &= 0,\end{aligned} \quad (13)$$

where  $L_n \equiv L\omega_{e,0}/v_{b,0}$  is the normalized gap width.

Equation (13) gives  $\chi$  as a function of  $L_n$ . The frequency is calculated from (11) and for a low-density beam with  $n_{b,0} \ll n_{e,0}$  it is

$$\omega = \frac{\omega_{e,0}}{\sqrt{1 - \frac{\omega_{b,0}^2}{\omega_{e,0}^2 \chi^2}}} \approx \omega_{e,0} \left( 1 + \frac{n_{b,0}}{2n_{e,0}\chi^2} \right). \quad (14)$$

The wavenumbers  $k_{\pm}$  can be obtained from (12).

Function  $\chi(L_n)$  is complex with band structure, *i.e.* it changes abruptly at certain  $L_n = c + 2\pi l$ , where  $c$  is a constant and  $l$  is an integer. Indeed, in the limit of

$L_n \gg 1$ , the first two terms in (13) are dominant which gives the following approximate expression:

$$-i\chi L_n e^{-i\chi L_n} = 2L_n^2 e^{-iL_n}.$$

Here, we used the fact that  $|\chi| \ll 1$  and  $\text{Im}(\chi) > 0$ . The solution of this equation is the Lambert or productlog function [9]:

$$-i\chi L_n = W(2L_n^2 e^{-iL_n}). \quad (15)$$

This function has many branches, the branch selected must ensure the maximal growth rate. When parameters of the plasma, *e.g.* the discharge gap, change, a transition from one branch to another may occur and the instability growth rate will change abruptly.

Since  $\chi$  is complex and independent on  $n_{b,0}$ , it follows from (14) that the temporal growth rate of the instability is proportional to  $\omega_{e,0}(n_{b,0}/n_{e,0})$  unlike the growth rate of the resonant perturbation  $k \approx \omega_{e,0}/v_{b,0}$  in a periodic system proportional to  $\omega_{e,0}(n_{b,0}/n_{e,0})^{1/3}$  [1].

The analytical solution is verified by fluid and particle-in-cell (PIC) simulations described below.

### Fluid simulations

The fluid numerical model solves Eqs. (1)-(3). The densities in (1) are advanced using the SHASTA method [10]. The velocities in (2) are advanced using an upwind scheme [11]. The model demonstrates excellent agreement with the theory [1] in simulations of the instability of a cold beam in a cold plasma with periodic boundary conditions.

The fluid simulations are carried out with the following common parameters:  $n_{e,0} = 2 \times 10^{17} \text{ m}^{-3}$ ,  $\omega_{e,0} = 2.52 \times 10^{11} \text{ s}^{-1}$ , beam energy 50 eV and beam velocity  $v_{b,0} = 4.2 \times 10^6 \text{ m/s}$ , the numerical grid cell size is  $1.3 \mu\text{m}$ , the time step is 0.9 fs. The selected values of spatial and temporal steps ensure stability of the SHASTA algorithm. The resonant beam wavelength  $\lambda_b \equiv 2\pi v_{b,0}/\omega_{e,0}$  is 1.044 mm for these plasma parameters. Initially, the bulk electron flow velocity is given a harmonic perturbation  $\delta v_e = \delta v_{e,0} \sin(x\omega_{e,0}/v_{b,0})$  with the wavelength corresponding to the resonance in a periodic or an infinite plasma, the amplitude of the perturbation is very small,  $\delta v_{e,0} = 0.1 \text{ m/s}$ .

The oscillations have the wavelength of the initial perturbation during only the first few periods. The initial oscillation pattern corresponds to a standing wave. As the instability develops, the standing wave transforms to a propagating wave, see Fig. 1a. This process is accompanied by the shrinking of the wavelength, compare the density perturbation profiles at three consecutive times in Fig. 2. At the initial phase of the instability, the perturbations propagate with the original beam velocity, see Fig. 1a. At the asymptotic stage given by Eq.(4) with

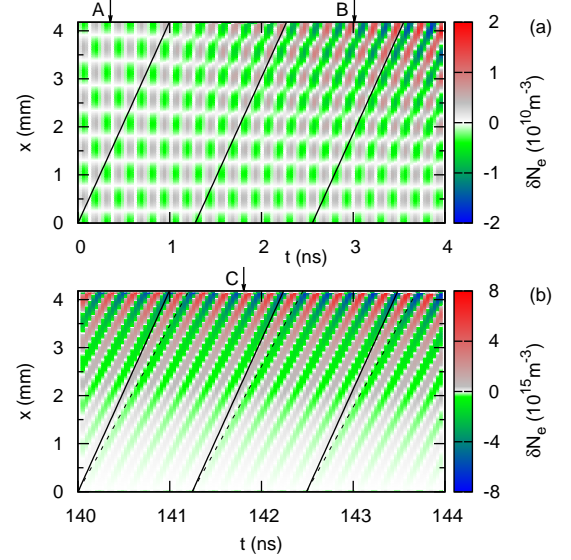


FIG. 1: Evolution of the bulk electron density perturbation in time and space in fluid simulation with  $L = 4\lambda_b$  and  $\alpha = 0.0006$ . Panels (a) and (b) correspond to the very beginning of the fluid simulation (a) and to the asymptotic constant growth stage (b); the corresponding temporal growth of the electric field amplitude is shown by the red curve in Fig. 3. Solid black lines in (a) and (b) represent propagation with the unperturbed beam velocity. Dashed black lines in (b) represent phase velocity of the wave calculated as  $\text{Re}(\omega)/\text{Re}(k)$ , where  $\text{Re}(\omega) = 2.522 \times 10^{10} \text{ s}^{-1}$  and  $\text{Re}(k) = 7.288 \text{ mm}^{-1}$ . Arrows A, B, and C mark times  $t_A = 0.35 \text{ ns}$ ,  $t_B = 3.01 \text{ ns}$ , and  $t_C = 141.8 \text{ ns}$  when profiles shown in Figs. 2a, 2b, and 2c are obtained.

the spatial growth rate along the beam propagation, the wave phase velocity is noticeably lower than the velocity of beam propagation, compare the slope of the black dashed line with that of the black solid lines in Fig. 1b.

Simulation reveals that before the asymptotic state establishes, the temporal growth rate changes with time, see Fig. 3. Initially, the growth rate is large compared to the analytical value defined by Eqs. (14) and (13). Then it gradually decreases towards the asymptotic value predicted by the theory and it stays approximately constant for tens and even hundreds of plasma periods until the nonlinear stage of instability and its saturation occurs, see the red curve in Fig. 3. Note that the modification of the wavelength mentioned above stops when the instability reaches the asymptotic stage, which for the red curve in Fig. 3 occurs near 20 ns.

In order to investigate the dependence of the growth rate on plasma parameters, four simulation sets are discussed below. In set one, the ratio of the beam to plasma density is  $\alpha \equiv n_{b,0}/n_{p,0} = 0.00015$ , the size of the system  $L$  increases from  $\lambda_b$  to  $8.5\lambda_b$ . Set two is similar to set one but the beam density is higher,  $\alpha = 0.0006$ . In set three,  $L = 3.4\lambda_b$  is constant while  $\alpha$  changes from

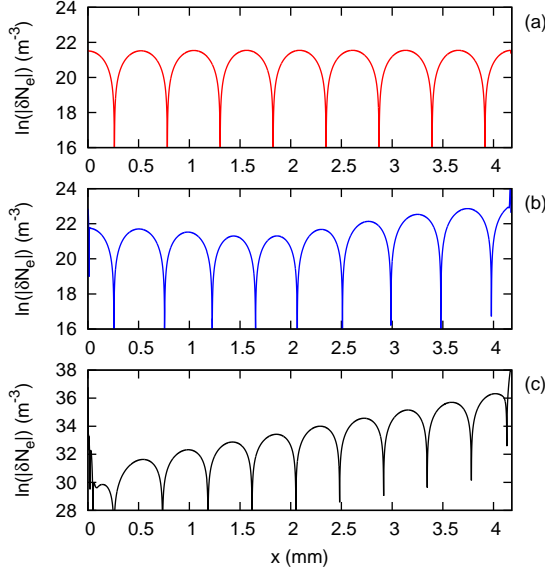


FIG. 2: Spatial profiles of bulk electron density perturbation obtained at  $t_A = 0.35$  ns (a),  $t_B = 3.01$  ns (b), and  $t_C = 141.8$  ns (c). Times  $t_{A,B,C}$  are shown by arrows A, B, and C in Fig. 1.

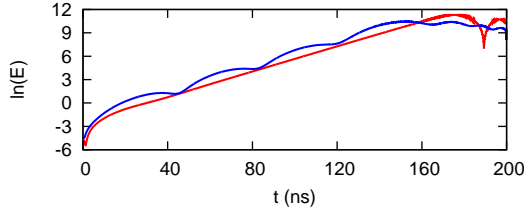


FIG. 3: Amplitude of electric field oscillations versus time in fluid simulations with  $\alpha = 0.0006$  and  $L = 4\lambda_b$  (red curve),  $L = 4.7\lambda_b$  (blue curve). The curves are obtained in the point with coordinate  $x = 3.55$  mm (red) and  $x = 4.34$  mm (blue).

0.0001 to 0.0006. The fourth set is similar to set three but  $L = 8.3\lambda_b$ .

In all simulations, the growth rates, the frequencies, and the wavenumbers are calculated during the asymptotic stage when the temporal growth rate is constant for a prolonged period of time, see the red curve in Fig. 3 for  $20 \text{ s} < t < 160 \text{ s}$ . In simulation sets one and two, for some values of  $L$  such a stage never appears, see the blue curve in Fig. 3. These values of  $L$  correspond to the gaps in the simulation data seen in Fig. 4.

Overall, there is an excellent agreement between the simulations and the theory. The dimensionless values of  $[\text{Re}(\omega) - \omega_{e,0}]/(\omega_{e,0}\alpha)$ ,  $\text{Im}(\omega)/(\omega_{e,0}\alpha)$ ,  $\text{Re}(k\lambda_b)$ , and  $\text{Im}(k\lambda_b)$  obtained in simulation sets one and two (red and black curves in Fig. 4) and by analytical solution of the theoretical dispersion relation (blue crosses in Fig. 4) are very close to each other and appear to be functions of the dimensionless system length only, as predicted by the an-

alytical solution given by Eqs. (12) and (14). These functions for  $\text{Re}(\omega)$ ,  $\text{Im}(\omega)$ , and  $\text{Re}(k)$  have band structure. Mathematically, it is the consequence of the presence of many branches in the Lambert function. The instability growth is given by the maximum growth rate value that changes from branch to branch when the gap size crosses some critical value, typically when  $L/\lambda_b$  approaches an integer, see Fig. 4. Similar band structure was also observed for the Pierce diode [7, 12]. Figure 4e shows the number of wave periods in the gap as a function of the gap length. In all cases, it is very close to an integer number, although not exactly:

$$\text{Re}(k)L/(2\pi) \simeq \lceil L/\lambda_b \rceil, \quad (16)$$

where  $\lceil x \rceil \equiv \text{ceiling}(x)$  is the smallest integer not less than  $x$ .

Since the shape of the functions is universal for various beam densities, it is reasonable to introduce approximate formulas which fit the numerical solution as follows:

$$\text{Re}(\omega) \approx \frac{\omega_{e,0}\alpha}{18} L_n \ln(L_n) [1 - 0.9 \cos(L_n + 0.4)], \quad (17)$$

$$\text{Im}(\omega) \approx \frac{\omega_{e,0}\alpha}{13} L_n \ln(L_n) \left[ 1 - 0.18 \cos\left(L_n + \frac{\pi}{2}\right) \right], \quad (18)$$

$$\text{Re}(k) \approx \frac{\omega_{e,0}}{v_{b,0}} \left[ 1.1 + \frac{1 + 2.5 \cos(L_n)}{1.1 L_n} \right], \quad (19)$$

$$\text{Im}(k) \approx \frac{\omega_{e,0}}{v_{b,0}} \frac{2 \ln(L_n) - 0.5}{L_n}. \quad (20)$$

The wavenumber and the spatial growth rate depend on the system length but are virtually insensitive to the beam density, see Fig. 5c and Fig. 5d. The temporal growth rate is approximately linearly proportional to the relative beam density  $\alpha$ . The linear law holds especially well for short systems, see the red curve in Fig. 5b and compare red and black curves for  $L/\lambda_b < 6$  in Fig. 4b. For longer systems, however, deviation from the linear law becomes noticeable.

### Kinetic simulation

Kinetic simulations are carried out with the EDIPIC 1D3V particle-in-cell (PIC) code [14]. The code is modified to reproduce conditions of the fluid simulations. The ions form an immobile background, the boundaries have zero potential. The bulk electrons are reflected specularly from the boundaries. The beam electrons penetrate through the boundaries freely. The initial plasma density and the beam energy are the same as in the fluid simulations. Collisions are omitted. Two simulations are carried out with  $L = 8.3\lambda_b$ ,  $\alpha = 0.0006$  but different

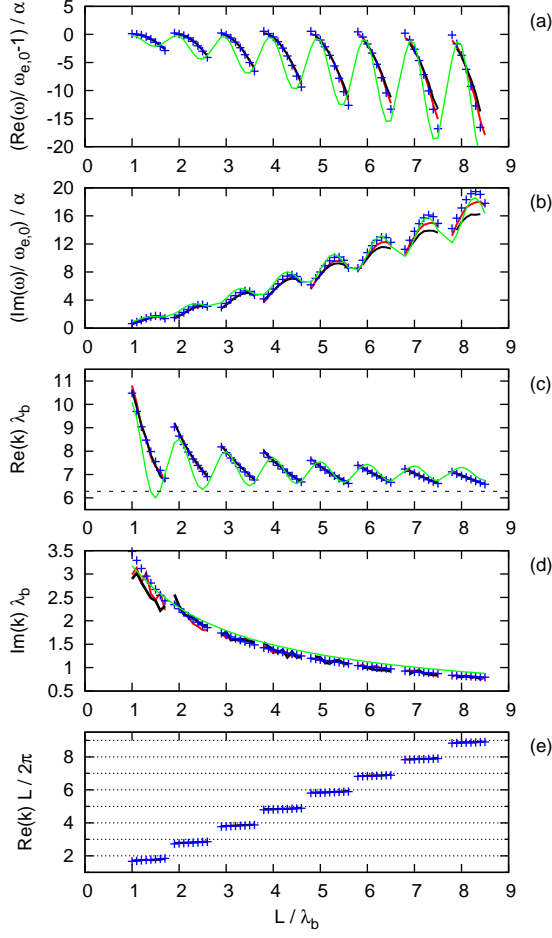


FIG. 4: Frequency (a), temporal growth rate (b), wavenumber (c), spatial growth rate (d), and the number of wave periods per system length (e) versus the length of the system. The blue crosses mark values obtained by analytical solution given by equations (13), (14), and (12). Solid red and black curves represent values obtained in fluid simulations with  $\alpha = 0.00015$  (red) and  $\alpha = 0.0006$  (black). Solid green curves are values provided by fitting formulas (17), (18), (19), and (20). In (c), the black dashed line marks the resonant wavenumber.

number of particles per cell. One simulation has 10000 particles per cell. The other simulation has 2000 particles per cell. Below these simulations are referred to as 10k and 2k simulations, respectively.

PIC simulations start with a significant level of statistical noise which is few orders of magnitude higher than the initial perturbation induced in the fluid simulations above. At the same time, the amplitudes of nonlinear saturation of the instability in PIC and fluid simulations are close to each other. As result, the time when the oscillations grow from the initial noise level to the saturation in PIC simulation is much shorter than that in a fluid simulation. Moreover, at the initial stage the growth rate gradually decreases which furthermore limits

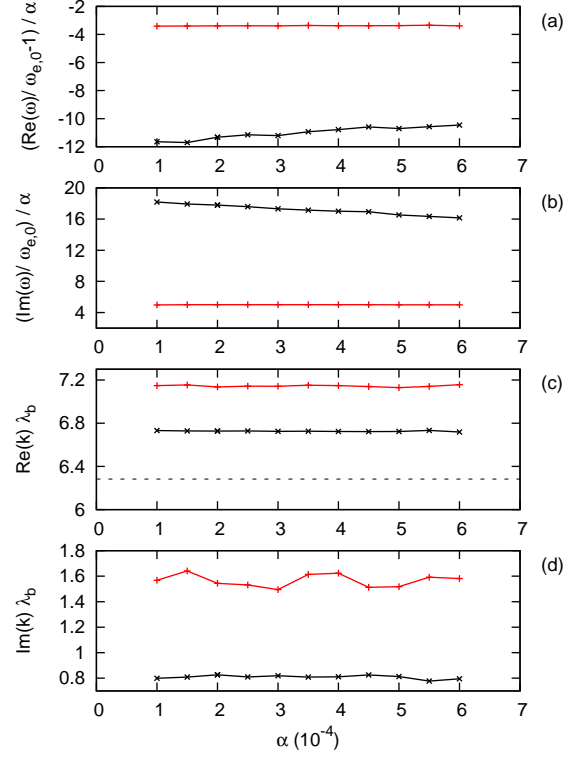


FIG. 5: Frequency (a), temporal growth rate (b), wavenumber (c), and spatial growth rate (d) versus the ratio of the beam and bulk electron densities in fluid simulations with  $L = 3.4\lambda_b$  (red) and  $L = 8.3\lambda_b$  (black). In (c), the black dashed line marks the resonant wavenumber.

the duration of the asymptotic stage described by analytic solution. For example, in the 10k simulation, the asymptotic stage lasts from 10 ns to 20 ns while in the fluid simulation that stage occurs between 10 ns and 45 ns, compare the green and the red curves in Fig. 6. The short asymptotic stage in the 10k simulation still allows to calculate the temporal growth rate which appeared to be very close to the value obtained in fluid simulations. In the 2k simulation, however, the noise level is higher and the asymptotic stage is very short and barely detectable, see the blue curve in Fig. 6.

In summary, we have studied the development of the two-stream instability in a finite size plasma bounded by electrodes both analytically and making use of fluid and particle-in-cell simulations. We show that the instability reaches the asymptotic state when the wave structure has the same spatial profile and grows in time with a constant growth rate. The spatial structure of the wave is close to a standing wave but has a spatial growth along the beam propagation. We derived analytic expressions for the frequency, wave number and the spatial and temporal growth rates. Obtained analytic solution agrees well with the values given by fluid and particle-in-cell simulations.

*Acknowledgement:* This research was supported in

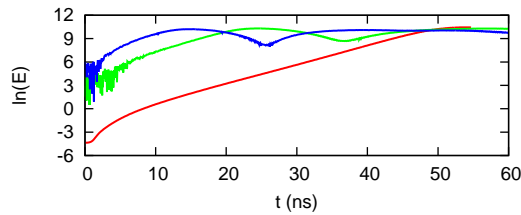


FIG. 6: Amplitude of electric field oscillations vs time in simulations with  $L = 8.3\lambda_b$  and  $\alpha = 0.0006$ . The curves represent fluid simulation (red), PIC simulation with 10000 particles per cell (green), and PIC simulation with 2000 particles per cell (blue).

part by U.S. Department of Energy and Air Force Office of Scientific Research. Authors acknowledge valuable discussions with Edward Startsev and Peter Ventzek.

- 
- [1] R. Briggs, *Electron-Stream Interaction with Plasmas*, MIT Press, 1964.
  - [2] S. Kainer, J. Dawson, R. Shanny, and T. Coffey, *Phys.*

- Fluids* **15**, 493 (1972).
- [3] I. J. Morey and R. W. Boswell, *Phys. Fluids B* **1**, 1502 (1989).
- [4] H. Gunell, J. P. V. N. Brenning, and S. Torven, *Phys. Rev. Lett.* **77**, 5059 (1996).
- [5] P. H. Yoon, T. Rhee, and C.-M. Ryu, *Phys. Rev. Lett.* **95**, 215003 (2005).
- [6] J.R. Pierce, *J. Appl. Phys.* **15**, 721 (1944).
- [7] A. Piel, “*Plasma Physics An introduction to Laboratory, Space and Fusion Plasmas*”, Springer-Verlag, Berlin 2010.
- [8] M. Rosenbluth, L. Pearlstein and G. Stuart, *Phys. Fluids* **6**, 1289 (1963).
- [9] R. M Corless, G. H. Gonnet, D.E.G. Hare, D. J. Jeffrey, D. E. Knuth, *Advances in Computational Mathematics* **5**, 329 (1996).
- [10] J. P. Boris, D. L. Book, *Journal of Computational Physics* **11**, 38 (1973).
- [11] “*Flux-Corrected Transport: Principles, Algorithms, and Applications*”, edited by D. Kuzmin, Rainald Löhner, Stefan Turek, Springer, 2005.
- [12] J. R. Cary and D. S. Lemons, *Journal of Applied Physics*, **53**, 3303 (1982).
- [13] A. I. Smolyakov, W. Frias, I. D. Kaganovich, and Y. Raitses, *Phys. Rev. Lett.* **111**, 115002 (2013).
- [14] D. Sydorenko, Ph.D., University of Saskatchewan (2006).